Heliyon 9 (2023) e13644

Contents lists available at ScienceDirect

Heliyon

journal homepage: www.cell.com/heliyon

Research article

In silico anti-SARS-CoV-2, antiplasmodial, antioxidant, and antimicrobial activities of crude extracts and homopterocarpin from heartwood of *Pterocarpus macrocarpus* Kurz.

Dwi Kusuma Wahyuni [a,b], Sumrit Wacharasindhu [c], Wichanee Bankeeree [a], Hunsa Punnapayak [a], Sehanat Prasongsuk [a,b,*]

[a] *Plant Biomass Utilization Research Unit, Department of Botany, Faculty of Science, Chulalongkorn University, Bangkok, 10330 Thailand*
[b] *Department of Biology, Faculty of Science and Technology, Universitas Airlangga, Surabaya, East Java, 60115, Indonesia*
[c] *Department of Chemistry, Faculty of Science, Chulalongkorn University, Bangkok, 10330, Thailand*

ARTICLE INFO

Keywords:
Anti-SARS-CoV-2
Antimicrobial
Antioxidant
Antiplasmodial
Homopterocarpin
Malaria
Pterocarpus macrocarpus Kurz.

ABSTRACT

Natural products play an essential role in new drug discovery. In the present study, we determined the anti-SARS-CoV-2 (severe acute respiratory syndrome-related coronavirus-2), antioxidant, antiplasmodial, and antimicrobial activities of *Pterocarpus macrocarpus* Kurz. heartwood and structurally characterized the bioactive compounds. *P. macrocarpus* Kurz. heartwood was macerated with *n*-hexane, ethyl acetate, and ethanol, respectively, for 7 days, three times. The compounds were isolated by recrystallization with *n*-hexane and evaluated by thin-layer chromatography (TLC), gas chromatography-mass spectrophotometry (GC-MS), Fourier transform infrared spectroscopy (FITR), and nuclear magnetic resonance (NMR) spectroscopy. Ethyl acetate, ethanol, *n*-hexane extracts, and homopterocarpin exhibited antiplasmodial activity at 1.78, 2.21, 7.11, and 0.52 μg/ml, respectively, against *P. falciparum* 3D7 with low toxicity (selectivity index/SI $\geq$ 28.46). GC-MS identified compound showed *in silico* anti-SARS-CoV-2 binding affinity with stigmasterol and SARS-CoV-2 helicase of −8.2 kcal/mol. Ethyl acetate extract exhibited the best antioxidant activity against DPPH (0.76 $\pm$ 0.92 μg/ml) and ABTS (0.61 $\pm$ 0.46 μg/ml). They also demonstrated antimicrobial activity against *B. subtilis*, ethanol and ethyl acetate extracts against *E. coli* and *C. albicans*, and ethanol extract against *S. aureus* with diameter zone of inhibition of more than 1 cm. The results highlighted antiplasmodial activity of extracts and homopterocarpin from *P. macrocarpus* Kurz. heartwood and its potent binding *in silico* to anti-SARS-CoV-2 proteins with low toxicity. This study also confirmed that extracts exhibited antioxidant and antimicrobial activities. Further studies are needed to assess the safety and clinical trial of *P. macrocarpus* Kurz. for development as new drug candidate.

1. Introduction

Severe acute respiratory syndrome-related coronavirus-2 (SARS-CoV-2) is currently a serious worldwide health problem, with more than 205 million people afflicted with this virus and the occurrence of more than 4 million deaths. To reduce the harmful

* Corresponding author. Plant Biomass Utilization Research Unit, Department of Botany, Faculty of Science, Chulalongkorn University, Bangkok, 10330 Thailand
E-mail address: sehanat.p@chula.ac.th (S. Prasongsuk).

https://doi.org/10.1016/j.heliyon.2023.e13644
Received 6 April 2022; Received in revised form 27 January 2023; Accepted 6 February 2023
Available online 10 February 2023

sequelae of this infection, efforts are underway to identify agents for preventive, supportive, and therapeutic care against SARS-CoV-2 [1]. Moreover, the emergence and spread of drug- or antimicrobial-resistant pathogens is another major threat that has increased the morbidity and mortality of infectious diseases, especially for artemisinin-resistant *Plasmodium falciparum* malaria [2]. These strains are resistant to nearly all available antimalarial drugs, which reinforces the need to identify new antimalarial and antimicrobial agents. Researchers are currently exploring the efficacy of phytochemicals from medicinal plants as a source of active compounds to reduce the time and cost of developing new synthetic drugs [3].

Herbal medicine and therapy were the best options according to traditional folklore. WHO estimates that around 80% of the world's population uses herbal medicines to treat health problems because they have many benefits, such as low costs, positive complementary effects, and negligible side effects [4]. Many plants that have been used in traditional medicine exhibit antiviral properties. The anti-SARS-CoV-2 activity of plant extracts and their components has been evaluated, such as bioactive compounds from *Centella asiatica* [5], *Vitis amurensis* [6], and *Boesenbergia rotunda* [7]. Some reports showed that many plants have been explored for combating COVID-19 [8, 9]. They have been also explored in many bioactivities studies, including antioxidant and antimicrobial activity [10–14]. Many plants have also been used in traditional medicine exhibited antiviral activity, such as *Artocarpus sericicarpus, Artocarpus dadah, Eusideroxylon zwageri,* and *Neolitsea cassiaefolia,* having potential inhibition for anti-hepatitis C virus (anti-HCV) with IC_{50} range 0.08 ± 0.05 to 12.01 ± 0.95 μg/mL [15]. In traditional medicine, some herbs are important multipurpose, such as *Ziziphus mucronata* Willd. [16], *Sonchus arvensis* L. [17], and *Glycyrrhiza glabra* L. [18].

Pterocarpus macrocarpus Kurz. belongs to Fabaceae, which primarily grows in Laos, Thailand, Myanmar, and Vietnam. The benefits of *P. macrocarpus* Kurz. is associated with its heartwood, which provides visual enjoyment and psychological pleasure because of its unique woody flavor [19]. In addition, medicinal properties are associated with the extracts from this plant including human blood circulatory, antimicrobial [20], detoxification [21], Alzheimer's disease, anti-spasmodic, anticancer [22], immunomodulatory [23], and insecticide activities [24]. Although *P. macrocarpus* Kurz. is known for its pharmaceutical benefits, the chemical structures, and properties of its extracts against artemisinin-resistant *Plasmodium falciparum* malaria and SARS-CoV-2 remain to be explored.

In this report, we evaluated the biological activities of the extracts and the purified homopterocarpin from *P. macrocarpus* Kurz. heartwood, including the antioxidant, antimicrobial, and antimalarial activities, and used computational analysis to determine the potency of these extracts and homopterocarpin against SARS-CoV-2 proteins. Their activities were then compared with those of the bioactive commercial compounds. The cytotoxicity test of the extracts and homopterocarpin was also conducted.

2. Materials and methods

2.1. Plant material collection and identification

P. macrocarpus Kurz. was obtained from a traditional market in Bangkok, Thailand. The sample was authenticated in the Plant Systematic Laboratory, Department of Biology, Faculty of Science and Technology, Universitas Airlangga. A voucher specimen was deposited in the Plant Systematic Laboratory, Department of Biology, Faculty of Science and Technology, Universitas Airlangga (No. PM.0210292021).

2.2. Extraction and phytochemical screening

The heartwood (1 kg) of *P. macrocarpus* Kurz. was air-dried, ground into powder (40 mesh size), and macerated sequentially in polar organic solvents including *n*-hexane, ethyl acetate, and ethanol. Each maceration was done for 7 days, 3 times at room temperature (28 ± 2 °C). The resulting extracts were filtered through filter paper, evaporated with a rotary evaporator at 60 °C to acquire a dry residue, weighed to calculate the yield of each extract, and stored at 4 °C. The crude extracts were screened for phytochemical content by standard methods including the Wilstatter "cyanidin" test for flavonoids, Mayer's test for alkaloids, the ferric chloride test for tannins, the Liebermann–Burchard test for terpenoids, and the foam test for saponins [25,26].

2.3. Isolation and structural analysis of bioactive compounds

The *n*-hexane extract of *P. macrocarpus* Kurz. was crystallized by dissolving 1 g of sample into 20 ml of *n*-hexane, shaking for 10 min, and incubating at 4 °C for 24 h. The crystals were separated by filtration through filter paper, weighed to calculate yield, and recrystallized. The process was repeated until the color of the crystals had become white. The thin-layer chromatography (TLC) with a mixture of *n*-hexane: ethyl acetate (4:1 v/v) as a mobile phase was used to separate the chemical constituents of the *n*-hexane extract before and after crystallization. The samples were dissolved in *n*-hexane and spotted (5 μL, equivalent to crude extract weight of 250 μg of sample) on a silica gel precoated plate. The plate was developed in vanillin-sulfuric acid and heated (105 °C) until purple-blue nodes were revealed on the plate as terpenoids [27]. Gas chromatography-mass spectrophotometry (GC-MS) was used to establish compound profiles from the *n*-hexane extract during the recrystallization steps. GC-MS analysis was performed using an Agilent GC-MSD (Agilent 19091S–433UI) equipped with a capillary column (30 m × 250 μm × 0.25 μm) and a mass detector was operated in electron impact (EI) mode with full scan (50550 amu). Helium was used as the carrier gas at a flow rate of 3 ml/min with a total flow rate of 14 ml/min. The injector was operated at 280 °C and the oven temperature was programmed at an initial temperature of 60 °C and increased 3 °C per minute to obtain a final temperature at 250 °C. The peaks in the chromatogram were identified based on their mass spectra. The compounds were analyzed using a nuclear magnetic resonance (NMR), JEOL JNM-ECS instrument, at 400 MHz in chloroform ($CDCl_3$) solvent, including the proton (^1H), carbon (^{13}C), heteronuclear multiple bond correlation (HMBC), and heteronuclear single quantum

correlation (HMQC) NMR spectra. The melting point was analyzed using a melting point tester (Stuart SMP30) and confirmed by Fourier transform infrared spectroscopy (FITR, Shimadzu IR Tracer 100).

2.4. In silico anti-SARS-Cov-2

2.4.1. Protein and ligand sample preparation

The proteins used in this study involved in entry, replication, and assembly of the SARS-CoV-2 virus in humans. The crystal structures of these proteins were obtained from the protein data bank (PDB), (https://www.rcsb.org), such as helicase (PDB ID 6ZSL), receptor binding domain (RBD) of spike glycoprotein (RBD-spike; PDB ID 6LZG), RNA dependant RNA polymerase (RdRp; PDB ID 6M71), and main protease (Mpro; PDB ID 7ALH) were identified as potential drug targets in this study. Molnupiravir (control with compound identification number (CID) 145996610) and PF-07321332 (control 2; CID 155903259) were used as control anti-SARS-CoV-2 drugs. To evaluate anti-SARS-CoV-2 activity, the three-dimensional structures of the identified compounds from the *n*-hexane extracts of *P. macrocarpus* Kurz., including butylated hydroxytoluene (CID 31404), 2-naphthalene methanol (CID 74128), homopterocarpin (CID 101795), pterocarpin (CID 1715306), campesterol (CID 173183), γ-sitosterol (CID 133082557), and stigmasterol (CID 5280794), were downloaded from PubChem database (https://pubchem.ncbi.nlm.nih.gov). The compounds (or ligands) were subjected to energy minimization using the PyRx 0.9.9 tool to increase the flexibility and optimize binding. The native ligands were then removed through sterilization by PyMol version 2.5 [28]. The drug-likeness of these compounds was analyzed using Lipinski's rule of five on the SCFBIO web server (http://www.scfbio-iitd.res.in/software/drugdesign/lipinski.jsp). The rule requires a molecular mass >500 Da, high lipophilicity <5 Da, hydrogen bond donor <5 Da, and a hydrogen bond acceptor <10 Da [29]. The compounds that were identified as drug candidates with drug-like molecule properties were selected for further analysis [30].

2.4.2. Molecular docking simulation

The docking of selected compounds to target proteins was performed using PyRx version 0.9.9 software. The docking type was screened with a control molecule to ignore the functional side of the target protein, while the analysis focused on the binding energy. The binding energy was expressed as binding affinity (kcal/mol), which is the energy formed when a molecule interacts with another molecule. This energy indicates the level of bonding activity and the interaction pattern with a ligand [31].

2.4.3. Molecular interaction analysis

BIOVIA Discovery Studio 2017 software was used to analyze the interactions and positions of chemical bonds in the docked molecular complex. Weak bonds consisting of hydrophobic, Van der Waals, hydrogen, electrostatic, and -alkyl are shown by the software. Weak bonds are formed when ligands and proteins interact to initiate specific biological responses, such as activation and inhibition. Pocket binding domains on target proteins have a key role in this regard because they consist of specific amino acids [32]. The results of the molecular docking simulation in this study were displayed by PyMol software (https://pymol.org/2/), the structure of the ligand-protein molecules consisted of cartoons, surfaces, and sticks that underwent staining selection [33].

2.5. In vitro antioxidant activity

2.5.1. The 2,2-diphenyl-1-picryl-hydrazyl-hydrate (DPPH) inhibition assay

The DPPH inhibition assay was done according to Prieto [34] with modifications. Samples (100 μl) at different concentrations from 1.075 to 200 μg/ml in methanol were mixed with 100 μl DPPH reagent (0.2 mM) and incubated for 30 min at room temperature. Ascorbic acid and trolox were used as positive controls. The inhibition of DPPH was measured at 517 nm by the microplate reader (Thermo Scientific, USA). The percentage of DPPH inhibition was calculated by the equation (Equation (1)):

$$(A_{control}\text{-}A_{sample}) / A_{control} \times 100\% \quad (1)$$

Where A_{sample} is the absorbance from the mixture of DPPH reagent and the sample, whereas $A_{control}$ is the absorbance from the DPPH reagent. The percentage of inhibition at each concentration was plotted and regressed linearly to obtain the half-maximal inhibitory concentration (IC_{50}) value.

2.5.2. The 2,2'-azino-bis (3-ethylbenzthiazoline-6-sulphonic acid) (ABTS) inhibition assay

The ABTS inhibition assay was conducted according to the method of Fu et al. [35]. The ABTS reagent was prepared by mixing 7 mM ABTS solution with 2.4 mM potassium persulphate solution and stored at room temperature for 12–16 h in the dark. Then, the absorbance of the solution at 734 nm was measured (0.70–0.72). The sample (100 μl) at different concentrations from 1.075 to 200 μg/ml in methanol was mixed with 100 μl ABTS reagent. Ascorbic acid and trolox were used as positive control. The absorbance was measured at 734 nm after incubating for 5 min in the dark at room temperature by the microplate reader (Thermo Scientific, USA). The percent inhibition and IC_{50} value were calculated as described for the DPPH inhibition assay.

2.6. In vitro antimalarial assay

An *in vitro* antimalarial assay using cultures of *Plasmodium falciparum* strain 3D7 (Trager and Jensen 1972) was carried out, which was adapted from Wahyuni et al. [36]. The composition of the medium included human O red blood cells, 5% hematocrit in Roswell

Park Memorial Institute 1640 (RPMI 1640) (Gibco BRL, USA), 22.3 mM N-2-hydroxyethylpiperazine-N-2-ethanesulfonic acid (HEPES) (Sigma), hypoxanthine, sodium bicarbonate ($NaHCO_3$), and 10% human O^+ plasma. Chloroquine diphosphate was used as a positive control. Sample (1 mg) was dissolved in 100 μl of dimethyl sulfoxide (DMSO), 10 mg/ml, and used as a stock solution from which serial dilutions were prepared. The parasites used in this test were synchronous (ring stage) with ±1% parasitemia (5% hematocrit). Test solution (2 μl) at various concentrations was placed into each wheel (96 wheels) and 198 μl of the parasite was added (the final concentration of the test material was 100 μg/ml, 10 μg/ml, 1 μg/ml, 0.1 μg/ml, and 0.01 μg/ml). The test well was placed into the chamber and exposed to a gas mixture (O_2 5%, CO_2 5%, and N_2 90%). The chamber containing the test wells was incubated for 48 h at 37 °C. The cultures were then harvested, and a thin blood film was prepared by 20% Giemsa staining. The number of infected erythrocytes per 1000 normal erythrocytes was counted under a microscope (1000X). The data was used to calculate the percent growth and percent inhibition using the following formulas (Equations (2) and (3)):

$$\% \text{ Growth} = \% \text{ Parasitemia} - D0 \quad (2)$$

$$\text{Percent inhibition} = 100\% - [(Xu/Xk) \times 100\%] \quad (3)$$

Where D0 is the percentage of growth at the 0-h, whereas Xu and Xk are the percentage of growth in the test solution and negative control, respectively. Based on the percent inhibition data, statistical analysis was carried out using Probit analysis of the SPSS version 20 program to determine the IC_{50} value or the concentration of the test material that inhibits parasitic growth by 50%.

2.7. In vitro cytotoxicity assay

A tetrazolium (MTT) cytotoxicity assay was carried out *in vitro* on hepatocyte-derived cellular carcinoma cell line (Huh7it-1 cells) using 3-(4,5-dimethylthiazol-2-yl)-2,5-diphenyltetrazolium bromide as described by Fonseca et al. [37] and Ferreira et al. [38]. The Dulbecco's modified Eagle's medium (DMEM) medium was supplemented with 3.7 g of sodium bicarbonate ($NaHCO_3$) and adjusted to a pH of 7–7.2. A complete medium was made from 500 ml of DMEM media containing 50 ml of fetal bovine serum (FBS), 5 ml of nonessential amino acid (NEAA), and 6 ml of penstrep (penicillin-streptomycin) was used in this study. The cells at a concentration of 2.5×10^4 per well were distributed into 96 wells, except for control well. The samples (100 μL) were dissolved in DMSO and then diluted to various concentrations (0.1, 0.5, 1, 5, 10, 50, 100, 500, and 1000 μg/ml). The cells were incubated at 37 °C under an atmosphere of 5% of carbon dioxide and 95% humidity for 48 h, after which 15 μL of 5 mg/mL MTT solution (thiazolyl blue tetrazolium bromide, Sigma-Aldrich Chemie GmbH, Steinheim, Germany) in phosphate saline buffer (PBS) to each well. The cultures were incubated for 4 h. Next, the solution was removed with 100 μL DMSO to solve the precipitated. The assay was done in duplicate wells. The viability of the cells was determined by measuring the absorbance at 560 nm and 750 nm with a multiplate reader. The percentage of cell viability was calculated using the formula (Equation (4)):

$$\% \text{ viability: } (A_{sample}/A_{control}) \text{ x}100\% \quad (4)$$

where A_{sample} was absorbance at 560 nm–750 nm and $A_{control}$ is the absorbance of DMEM medium. The half cytotoxic concentration (CC_{50}) was determined by plotting the percent cell viability and regressing linearly using Microsoft Excel version 20.0 (IBM Corporation, Armonk, NY, USA).

2.8. Selectivity index (SI)

The SI value was calculated by comparing the IC_{50} value of the extract with that of *P. falciparum* strain 3D7. The SI was used to describe the selective activity of the extract against *P. falciparum* strain 3D7 compared with the results of its cytotoxicity on human hepatocyte cells [39].

2.9. Antimicrobial assay

The well diffusion method was performed to analyze antimicrobial activity against representatives from gram-positive bacteria (*Bacillus substilis* TISTR 1248 and *Staphylococcus aureus* ATCC 25923), gram-negative bacteria (*Escherichia coli* ATCC 25922), and yeast (*Candida albicans* ATCC 10231) [40]. Nutrient agar media was used to culture the bacteria, whereas potato dextrose agar was used for cultivating yeast. The 30 mL sterilized medium was poured into sterile Petri plates (Ø = 10 cm) and the 100 μL of inoculate (OD = 0.1) from each strain was spread onto the agar plates after solidification. A stock solution of extract was prepared and serially diluted (25% and 50%). The well, 5 mm in diameter, was made in the solidified medium. Twenty percent of DMSO was used as negative control. Chloramphenicol and nystatin were used as positive controls, for antimicrobial and antifungal respectively. All wells were filled with 30 μL of extract and control. Antibacterial activity was evaluated by measuring the diameter of the inhibition zone around the well. The percentage of inhibition (PI) was calculated as follows (Equation (5)):

$$PI = \text{the inhibition zone of the sample (cm) / the zone of positive control (cm)} \times 100\% \quad (5)$$

2.10. Data analysis

Data are expressed as the mean ± standard deviation. Probit analysis was used to calculate the IC_{50} values for *in vitro* antimalarial activity using IBM SPSS Statistics for Windows, version 20.0 (IBM Corporation, Armonk, NY, USA) [27]. The IC_{50} values for *in vitro* antioxidant and cytotoxicity were calculated by linear regression using Microsoft Excel version 20.0 (The Microsoft Corporation, Redmond, Washington, USA) [34,36,38].

3. Results and discussion

3.1. The yield of extracts and phytochemical screening

Dried heartwood from *P. macrocarpus* Kurz. was sequentially extracted with different polar organic solvents. One kilogram of sample yielded 2.5 ± 0.3, 10.2 ± 0.2, and 42.9 ± 0.3 g of extract from the *n*-hexane, ethyl acetate, and ethanol fractions, respectively. According to phytochemical analysis, each fraction contained flavonoid, alkaloid, terpenoid, and as secondary metabolites at different amounts, whereas phenolics were found in the ethyl acetate and ethanolic fraction, and then saponins were only found in the ethanolic fraction (Table 1). Some studies showed alkaloids, terpenoids, flavonoids, and saponin were produced by plants of Pterocarpus, however, there was no report for alkaloids compound from *P. macrocarpus* Kurz [41,42]. Morimoto et al. [24] reported that *P. macrocarpus* Kurz. contained flavonoids and terpenoids. Phytochemical screening on *P. mildbraedii* leaves revealed alkaloids, flavonoids, tannins, terpenoids, and saponins [43]. The *n*-hexane extract contained an abundance of terpenoids. Based on the previous study, *n*-hexane also revealed pterocarpan as major compound [20,24]. Therefore, crude extracts from the *n*-hexane fraction were selected for the isolation of bioactive compounds, for anti-viral screening (*in silico* anti-SARS-Cov2) and for antiplasmodial assay.

3.2. Isolation and structural analysis of bioactive compounds

Recrystallization was performed to isolate the bioactive compounds. The yield, color, and number of spots on TLC plates from each cycle of recrystallization are listed in Table 2. The effectiveness of this isolation technique may be observed by the reduction of spots on the TLC from 6 (1st cycle) to 3 spots (2nd – 4th cycle), until one spot (5th cycle). The different retention factor (Rf) values for every stain indicated the diversity of the compounds [44]. The yield of each cycle showed varied of weight. The highest white crystals that yielded 596 mg/g of crude extract were obtained at the 5th cycle and the single spot with an Rf value of 0.69 was also identified by TLC (Supplementary Data I). The results indicated a high purity of the compound. Based on the GC-MS analysis, the compound is homopterocarpin as major compound (Table 3). This report agreed with GC-MS analysis result by Chen et al. [22]. Morimoto et al. [24] also reported that homopterocarpin is major compound of *P. macrocarpus* Kurz.

A GC-MS chemical analysis was used to identify the diverse compounds in the *n*-hexane extract from the four cycles of recrystallization. A total of 7 compounds were identified from the first crystallization, 3 from the second, and only 2 compounds were identified from the third cycle. Of these, homopterocarpin and pterocarpin were found at each cycle as major components (Table 3, Fig. 1 (A-E), Supplementary data II). These compounds have been reported as bioactive molecules in previous studies [45–48].

The chromatogram profile of TCL and GC-MS analysis showed the chromatogram profile differences. It means there were differences in the distinguishing ability of the compound, however, TLC profile was analyzed based on the clear spots appeared after running with *n*-hexane:ethyl acetate (4:1) as the mobile phase. Then, the GC-MS analyzed the compound based on the boiling point of substance, so, GC-MS will show the metabolite profile of sample which is a thermally stable molecule [49].

The FTIR spectrum of the isolated products from the fifth recrystallization revealed absorption bands (cm^{-1}) for C–H alkane at 2949.16, 2908.65, and 2841.15; the C–H bending aromatic compound at 1876.74; C═C conjugated alkene at 1618.28; C═C cyclic alkene at 1587.42, O–H phenol at 1381.03 and 1344.38; C–O stretching alkyl aryl ether/aromatic ester/at tertiary alcohol 1197.79 and 1271.09; C═C stretching aliphatic ether at 1149.57 and 1130.29; and the C═C alkene at 973.40, 794.67, 723.31, and 682.80 (Supplementary data III). The integration of the ^{1}H NMR spectrum (Table 4) showed the presence of two aromatic rings in the benzene skeleton at δ_H 7.43 (1H, *d*, 8.6Hz), 6.64 (2H, *dd*, 8.6Hz; 2.5Hz), 6.47 (1H, *d*, 2.5Hz) and 7.13 (1H, *d*, 8.5Hz), 6.46 (2H, *dd*, 8.5Hz; 2.3Hz), 6.44 (1H, *d*, 2.3). The two ether cyclic groups were at δ_H 3.64 (3H, *t*, 11.0Hz), 4.25 (2H, *dd*, 11.0Hz; 5.3Hz), and 3.53 (*m*). The appearance of singlets at δ_H 3.77 (s) and 3.79 (s) confirmed the presence of two OCH_3 groups on the aromatic ring (Supplementary data IV). There were 17 carbon signals in the ^{13}C NMR spectrum (125 MHz, $CDCl_3$, based on HMQC and HMBC experiments; Table 4). Signals at δ_C 156.7 and 60.8 resulted from benzene carbons bonded to the ether group. The signals at δ_C 131.9, 109.3, 101.7, 39.6,

Table 1
Phytochemical screening of *Pterocarpus macrocarpus* Kurz. heartwood extracts.

No	Phytochemicals	*n*-Hexane[a]	Ethyl acetate	Ethanol
1	Terpenoids	+++	++	+
2	Flavonoids	+	++	+++
3	Alkaloids	++	++	++
4	Saponin	–	–	+
5	Phenolics	–	+	+++

[a] Note: + +, Strongly positive; +, Weakly positive; −, Not detected.

Table 2
The yield of crystals at each step of crystallization of the *n*-hexane extract of *Pterocarpus macrocarpus* Kurz. heartwood.

Cycle	Number of spots	Rf value for major spot	Yield (mg/g)	Color
1	6	0.125, 0.375, 0.563, 0.625, 0.688, 0.938	290 ± 5	orange
2	3	0.125, 0.688, 0.938	80 ± 2	orange
3	3	0.125, 0.688, 0.938	12 ± 10	orange
4	3	0.125, 0.688, 0.938	10 ± 10	orange
5	1	0.688	592 ± 30	white

Note: The data were represented as mean ± SD, n = 3. The TLC analysis used *n*-hexane:ethyl acetate (1:4) and sprayed vanillin sulfuric acid (105 °C) until purple-blue nodes were revealed on the plate as terpenoids. Rf = retention factor.

Table 3
Phytochemical components identified from GC-MS analysis of *Pterocarpus macrocarpus* Kurz. heartwood *n*-hexane extract at each crystallization cycle.

No.	Identified compound	Retention Time (min)	Relative area percentage (peak area relative to the total peak area (%))				
			hexane extract	Crystallization			
				1st	2nd	3rd	4th
1	Butylated hydroxytoluene	44.04	3.81	9.04			
2	2-Naphthalenemethanol	51.53	32.17	57.85	4.03		
3	Homopterocarpin	90.40	100.00	100.00	100.00	100.00	100.00
4	Pterocarpin	94.14	23.34	20.64	13.34	31.17	23.42
5	Campesterol	113.64	7.93	19.70			
6	Stigmasterol	114.64	21.24	43.03			
7	γ-sitosterol	116.50	27.87	55.97			

124.8, 106.4, 97.1, and 78.7 indicated an aromatic CH, whereas signals at δ_C 112.4 and 119.2 were assigned to aromatic carbons. The other two signals at δ_C 161.2 and 161.1 belong to a benzene carbon with methoxy groups. Two signals at δ_C 55.6 and C_9 55.5 were confirmed as methoxy carbons. The signal at δ_C 66.7 was a carbon ether cyclic with two hydrogen atoms. The data from the characterization of the compounds were compared with that reported in the literature [50]. Homopterocarpin exhibited white crystals and yielded 0.592 ± 0.003 g (0.059%, w/w). The melting point of this compound was 83.6 °C. Furthermore, a mass spectra analysis showed that the compound had an *m/z* of 284.1 and the molecular formula was $C_{17}H_{16}O_4$ (Fig. 2).

3.3. In silico anti-SARS-CoV-2 activity

The identified compounds include butylated homopterocarpin, pterocarpin, hydroxytoluene, 2-naphthalenemethanol, campesterol, γ-sitosterol, and stigmasterol from *P. macrocarpus* Kurz. *n*-hexane extract was used as the ligands to analyze their potential activity as drug-like molecules according to the Lipinski Rule of Five. All compounds that act as drug candidates may trigger the activity of the target protein if they satisfy more than two of the Lipinski rules (Table 5).

The results of a molecular docking simulation indicated that all the selected compounds had a higher negative binding affinity for each SARS-CoV-2 protein compared with that of molnupiravir (Control 1) and PF-07321332 (Control 2) (Table 6). Stigmasterol was the most effective compound predicted to bind with all SARS-CoV-2 proteins including helicase, RBD-spike, RdRp, and Mpro with negative binding affinities of −8.2, −7.8, −7.8 and −7.3 kcal/mol, respectively. Campesterol is another active compound that exhibited a more negative binding affinity with all target SARS-CoV-2 proteins compared with the two control drugs. The molecular docking simulation results were displayed in 3D with transparent surfaces, cartoon structures with the target proteins, and a ligand with stick views (Fig. 3A–D). The weak bonds in the molecular complex from the docking simulation consisted of hydrogen, alkyl, Van der Waals, hydrophobic, and electrostatic interactions. The presence of weak binding interactions can activate specific biological responses in proteins, such as inhibition through specific domains [51]. The seven bioactive compounds in this study could theoretically bind to specific protein domains through weak binding, such as alkyl, hydrogen, pi sigma, and Van der Waals interactions (Fig. 4A–D). The results suggest that each bioactive compound may inhibit SARS-CoV-2 protein activity.

3.4. Antioxidant activity

DPPH and ABTS assays were done to assess the antioxidant activities of the extracts. The IC_{50} values of the crude extracts prepared with each solvent are shown in Table 7. From lowest to highest, the IC_{50} values for ABTS were 0.61 ± 0.46, 0.75 ± 0.42, and 68.93 ± 4.34 μg/ml for the ethanol, ethyl acetate extract, and *n*-hexane extract, respectively, whereas the IC_{50} values for DPPH were 0.76 ± 0.92, 2.12 ± 0.97, and 27.70 ± 4.29 μg/ml for the ethanol, ethyl acetate extract, and *n*-hexane extracts, respectively. In addition, the IC_{50} of homopterocarpin was 194.90 ± 34.96 μg/ml for DDPH assay and 30.94 ± 8.00 μg/ml for the ABTS assay. Compared with the control, the IC_{50} for ethyl acetate and ethanol extracts were lower compared with that of trolox and ascorbic acid for both assays. The potent antioxidant activity of the crude extract of *P. macrocarpus* Kurz. was likely due to the presence of active ingredients with antioxidant activities, such as polyphenols and flavonoids, especially in the ethanolic and ethyl acetate crude extracts (Table 2) [52]. In

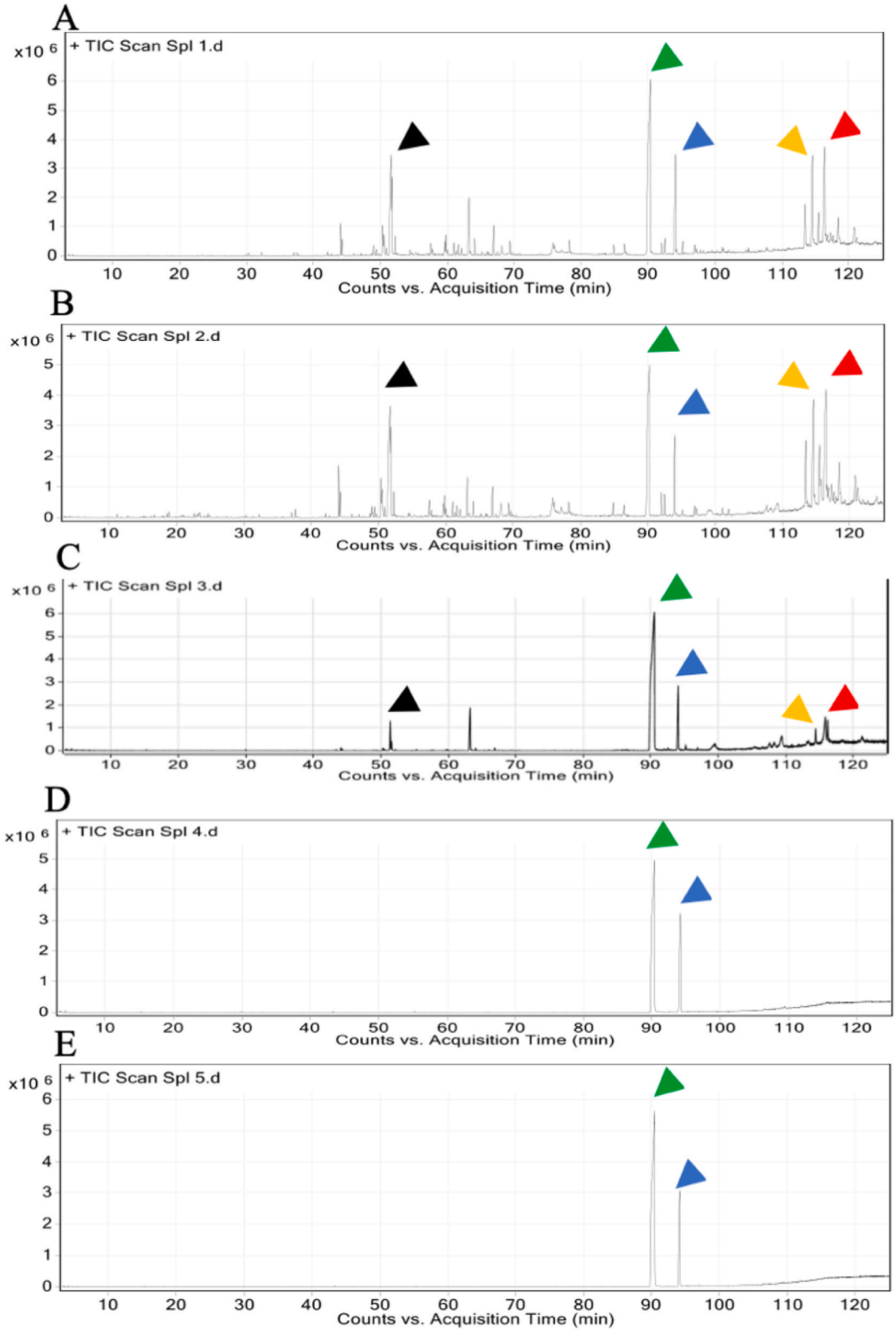

Fig. 1. Chromatogram of *n*-hexane extracts of *Pterocarpus macrocarpus* Kurz. heartwood at each crystallization cycle. A. *n*-hexane extract, B. first crystallization, C. second crystallization, D. third crystallization, E. fourth crystallization. black arrow: 2-naphthalenemethanol; green arrow: homopterocarpin; blue arrow: pterocarpin; yellow arrow: stigmasterol; red arrow: γ-sitosterol.

Table 4
The observed ^{1}H and^{13}C NMR homopterocarpin (3,9-dimethoxypterocarpan) compound in $CDCl_3$.

No. C	Homopterocarpin of *Pterocarpus macrocarpus* Kurz.		
	Type	δ_H (mult, *J* Hz)	δ_C
1	CH	7.43 (*d*, 8.6)	131.9
2	CH	6.64 (*dd*, 8.6; 2.5)	109.3
3	C	–	161.2
4	CH	6.47 (*d*, 2.5)	101.7
4a	C	–	156.7
6	CH2	3.64 (*t*, 11.0) 4.25 (*dd*, 11.0; 5.3)	66.7
6a	CH	3.53 (*m*)	39.6
6b	C	–	119.2
7	CH	7.13 (*d*, 8.5)	124.8
8	CH	6.46 (*dd*, 8.5; 2.3)	106.4
9	C	–	161.1
10	C	6.44 (*d*, 2.3)	97.1
10a	C	–	160.8
11a	CH	5.51 (*d*, 6.8)	78.7
11b	C	–	112.4
3-OCH_3	C–OCH3	3.77 (*s*)	55.6
9-OCH_3	C–OCH3	3.79 (*s*)	55.5

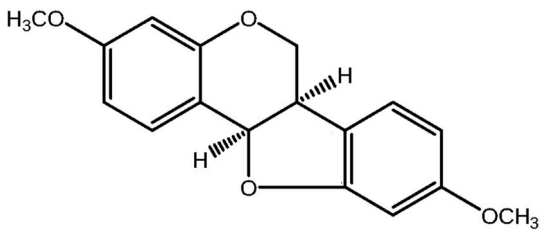

Fig. 2. The structure of homopterocarpin.

Table 5
Prediction results of target compound activity.

Compound	MW (Dalton)	LOGP	HBD	HBA	MR	Probability
Butylated hydroxytoluene	220.000	4.295	1	1	70.243	Drug-like molecule
2-Naphthalenemethanol	158.000	2.332	1	1	49.870	Drug-like molecule
Homopterocarpin	284.000	3.313	0	4	77.592	Drug-like molecule
Pterocarpin	298.000	3.033	0	5	77.163	Drug-like molecule
Campesterol	400.000	7.634	1	1	123.599	Drug-like molecule
γ-sitosterol	414.000	8.024	1	1	128.216	Drug-like molecule
Stigmasterol	412.000	7.800	1	1	128.122	Drug-like molecule

MW: *Molecular Weight*; LOGP: *High Lipophilicity*; HBD: *Hydrogen Bond Donor*; HBA: *Hydrogen Bond Acceptor*; MR: Molar Refractivity.

the previous study showed homopterocarpin from *Pterocarpus erinaceus* as antioxidant [48]. Compared to the other studies that have been previously reported as having high antioxidant compounds, the heartwood extract from *P. macrocarpus* Kurz. was lower than *Centella asiatica* L. leaf [53], plants, and callus of *Trifolium pratense* L. [54], and *Callisia fragrance* leaf juice [55].

3.5. In vitro antimalarial activity

The IC_{50} values of the crude extracts and homopterocarpin from *P. macrocapus* Kurz. at different doses are shown in Table 8. All natural products are considered to have antimalarial activity at IC_{50} values less than 10 μg/ml. The compounds with IC_{50} values less than 5 μg/ml are classified as exhibiting very active antimalarial activity, whereas IC_{50} values between 5 and 10 μg/ml are identified as active antimalarial agents [56]. The results indicated that the ethyl acetate extract exhibited the highest *in vitro* antimalarial activity with an IC_{50} value of 1.78 μg/ml, followed by the ethanol (2.21 μg/ml) and *n*-hexane extracts (7.11 μg/ml), whereas the IC_{50} of homopterocarpin was 0.52 μg/ml. Compared with other studies, the IC_{50} values for the *P. macrocarpus* Kurz. ethyl acetate extract was lower compared with that of the DCM extracts from *Commiphora africana* (A. Rich.) Engl. stem bark and *Dychrostachys cinerea* (L.) Wight & Arn. whole stem, which showed promising antiplasmodial activity with IC_{50} values of 4.54 ± 1.80 and 11.47 ± 2.17 μg/ml, respectively [3]. These results were lower compared with that of the ethanolic extracts from *Mussaenda erythrophylla,* including stem (29.6 ± 0.7 μg/ml) and leaves (3.7 ± 2.6 μg/ml), and *Mussaenda philippica* Dona Luz x *Mussaenda flava* leaves ethanolic extract (5.9 ±

Table 6
Simulation results of molecular docking with SARS-CoV-2 proteins.

Target	Ligand	Binding Affinity (kcal/mol)	AutoGrid (Å)
Helicase	Butylated hydroxytoluene	−6.3	Center X:-14.723 Y:30.321 Z:-66.631
	2-Naphthalenemethanol	−6.2	Dimensions X:91.761 Y:98.670 Z:106.327
	Homopterocarpin	−7.2	
	Pterocarpin	−7.7	
	Campesterol	−7.7	
	γ-sitosterol	−7.4	
	Stigmasterol	−8.2	
	Molnupiravir (Control 1)	−7.1	
	PF-07321332 (Control 2)	−7.1	
RdRp	Butylated hydroxytoluene	−5.9	Center X:119.72 Y:117.282 Z:117.111
	2-Naphthalenemethanol	−5.8	Dimension X:102.037 Y:108.952 Z:117.175
	Homopterocarpin	−6.5	
	Pterocarpin	−7.2	
	Campesterol	−7.6	
	γ-sitosterol	−7.1	
	Stigmasterol	−7.8	
	Molnupiravir (Control 1)	−6.8	
	PF-07321332 (Control 2)	−7.5	
M^{pro}	Butylated hydroxytoluene	−5.8	Center X:-26.283 Y:12.599 Z:63.866
	2-Naphthalenemethanol	−5.9	Dimension X:66.125 Y:72.942 Z:61.258
	Homopterocarpin	−6.3	
	Pterocarpin	−7.1	
	Campesterol	−7.7	
	γ-sitosterol	−7.6	
	Stigmasterol	−7.8	
	Molnupiravir (Control 1)	−6.7	
	PF-07321332 (Control 2)	−6.5	
RBD-Spike	Butylated hydroxytoluene	−5.6	Center X:-32.325 Y:27.893 Z:21.076
	2-Naphthalenemethanol	−5.6	Dimension X:48.156 Y:59.612 Z:56.346
	Homopterocarpin	−6.4	
	Pterocarpin	−7.1	
	Campesterol	−6.9	
	γ-sitosterol	−6.7	
	Stigmasterol	−7.3	
	Molnupiravir (Control 1)	−6.7	
	PF-07321332 (Control 2)	−6.6	

0.4 μg/ml) [57]. In addition, they were lower than *Pterocarpus erinaceus* Poir. leaf methanolic extract (IC_{50} = 14.63 μg/ml) [58]. Tajuddeen and Heerden [59] concluded that a bioactive compound is considered interesting and worthy of further investigation as an antimalarial agent if the IC_{50} is 3.0 μg/ml.

3.6. In vitro toxicity and selectivity index

In vitro toxicity was evaluated by the MTT assay using Huh7it-1 cells and the SI was calculated by comparing the cytotoxicity concentration at 50% (CC_{50}) and the IC_{50} of the antiplasmodial activity of the natural product. The CC_{50} of the crude *n*-hexane, ethyl acetate, ethanol extracts, and homopterocarpin were 202.38, 67.24, 512.48, and 49.93 μg/ml, respectively. Moreover, the selectivity indices for the *n*-hexane, ethyl acetate, and ethanol extracts of *P. macrocarpus* Kurz. heartwood and homopterocarpin were 28.46, 37.77, 231.89, and 96.02 respectively (Table 8). The drug's effectiveness and safety for treating the diseases were indicated by the SI value. Sinha et al. [60] described that the SI is investigational compound with relative effectiveness in inhibiting cell proliferation as compared to inducing cell death, so the SI value is preferred higher. The extract or fraction with SI values ranging from 10 to 313 was considered safe, regarding the effective concentration against a parasite and the toxic concentration toward human cells [40,60,61]. Therefore, all-natural products in this study were considered nontoxic to human cells and optimum selective antiplasmodial. Compared to other studies, extracts and homopterocarpin isolated from *P. macrocarpus* Kurz. showed higher SI than leaf extract of *Vernonia amygdalina* (Del.) [62], however, they are lower than malaria drug box (artesunate) [42].

3.7. Antimicrobial activity

The 5 microbial strains, including *Bacillus substilis* TISTR 1248, *Staphylococcus aureus* ATCC 25923, *Escherichia coli* ATCC 25922, and *Candida albicans* ATCC 10231, are used in this study as representatives of pathogenic bacteria and yeast which are commonly used for antimicrobial assay in a number of researches [63–65]. Antimicrobial tests were carried out with all crude extracts against bacteria and yeast (Table 9). All extracts showed active antibacterial activity against *B. substilis* TISTR 1248 with a PI of 39.50 ± 2.08%, 37.90 ± 0.29%, and 38.70 ± 3.27% for the *n*-hexane, ethyl acetate, and ethanol extracts, respectively. The ethyl acetate and ethanol extracts showed active antimicrobial activity against *C. albicans* ATCC 10231 (29.75 ± 1.53% and 27.40 ± 6.13% of inhibition, respectively)

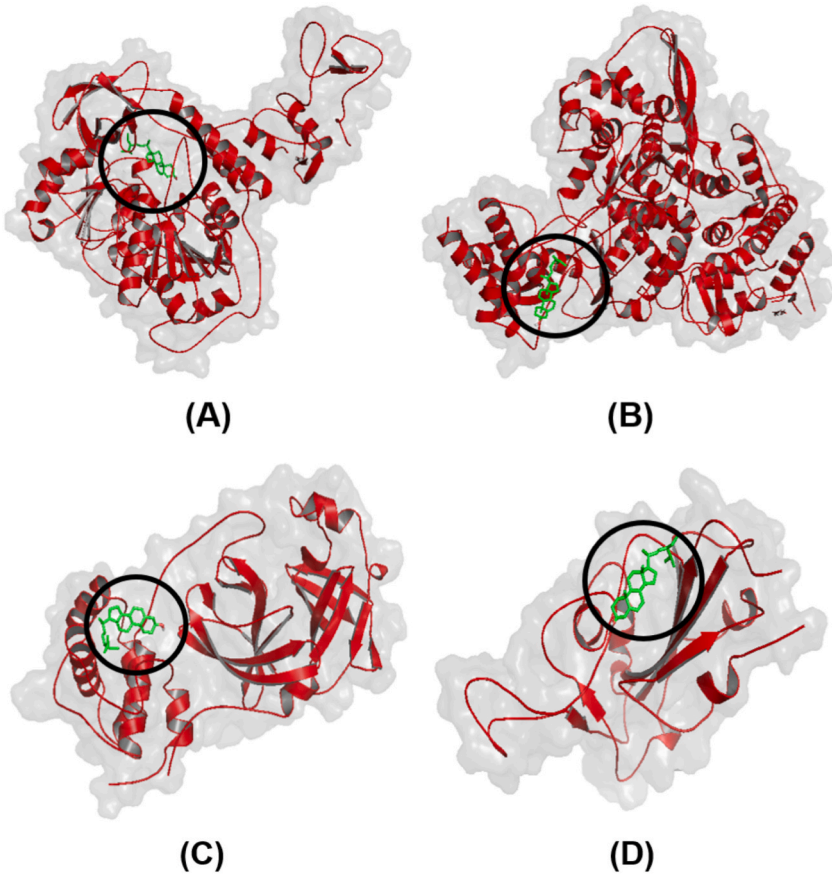

Fig. 3. The 3D visualization of the molecular docking results. Ligands are indicated by black circles (A) Stigmasterol_Helicase (B) Stigmasterol_RdRp (C) Stigmasterol_Mpro (D) Stigmasterol_RBD-Spike.

and *E. coli* ATCC 25922 (48.82 ± 7.48% and 57.76 ± 7.48%, respectively). Only ethanol extract has antimicrobial activity against *S. aureus* ATCC 25923 (44.78 ± 0.42%). Compared to other studies, diameter of inhibition zone of *P. macrocarpus* Kurz. extract was wider than *P. indicus* bark ethanolic extract against to *C. albicans, E coli*, and *S. aureus* [66]. The antimicrobial activity of the *P. macrocarpus* Kurz. extracts seemed to be related to the presence of active ingredients with antimicrobial activities (Tables 2 and 3). Jime'nez-Gonza'lez et al. [67] reported that pterocarpans have antifungal activity. However, in the present study, the antimicrobial activity of homopterocarpin was not determined because it did not show a significant inhibition zone against the tested microbes. These results are consistent with that of Cuellar et al. [68] in which homopterocarpin exhibited weak antimicrobial activity against *E. coli, S. aureus, B. cereus,* and *E. faecalis*.

It is important to note that the best antioxidant, antiplasmodial, and antimicrobial activities were found in the extracts from ethyl acetate and ethanol fractions of *P. macrocarpus* Kurz. compared with those of *n*-hexane extract and a purified compound, homopterocarpin. This result might be due to the high flavonoid contents in both ethyl acetate and ethanol extracts (Table 1), which have been reported to play an essential role in antimicrobial and antioxidant activities [65,69]. In contrast, terpenoids were highly found in *n*-hexane extract. Some compounds in this group have been reported to exhibit antiviral activity [70] that corresponded to the results of molecular docking of compounds from *n*-hexane extract against SARS-Cov-2 proteins in this study. Nevertheless, it is suggested that further *in vivo* experiments should be employed for ensuring the inhibitor's effectiveness and warranty against SARS-Cov-2.

4. Conclusion

This report highlighted the anti-SAR-CoV-2 and antiplasmodial activities of the extracts and homopterocarpin derived from *P. macrocarpus* Kurz. This study provided remarkable information regarding homopterocarpin isolation from *P. macrocarpus* Kurz. with high yield by crystallization. Moreover, all extracts from *P. macrocarpus* Kurz. heartwood showed antimicrobial and antioxidant activities with low toxicity as well. Thus, it could be expected to provide data for the further use of these extracts and homopterocarpin as drug candidates for infectious diseases therapy with positive complementary effects and no toxicity.

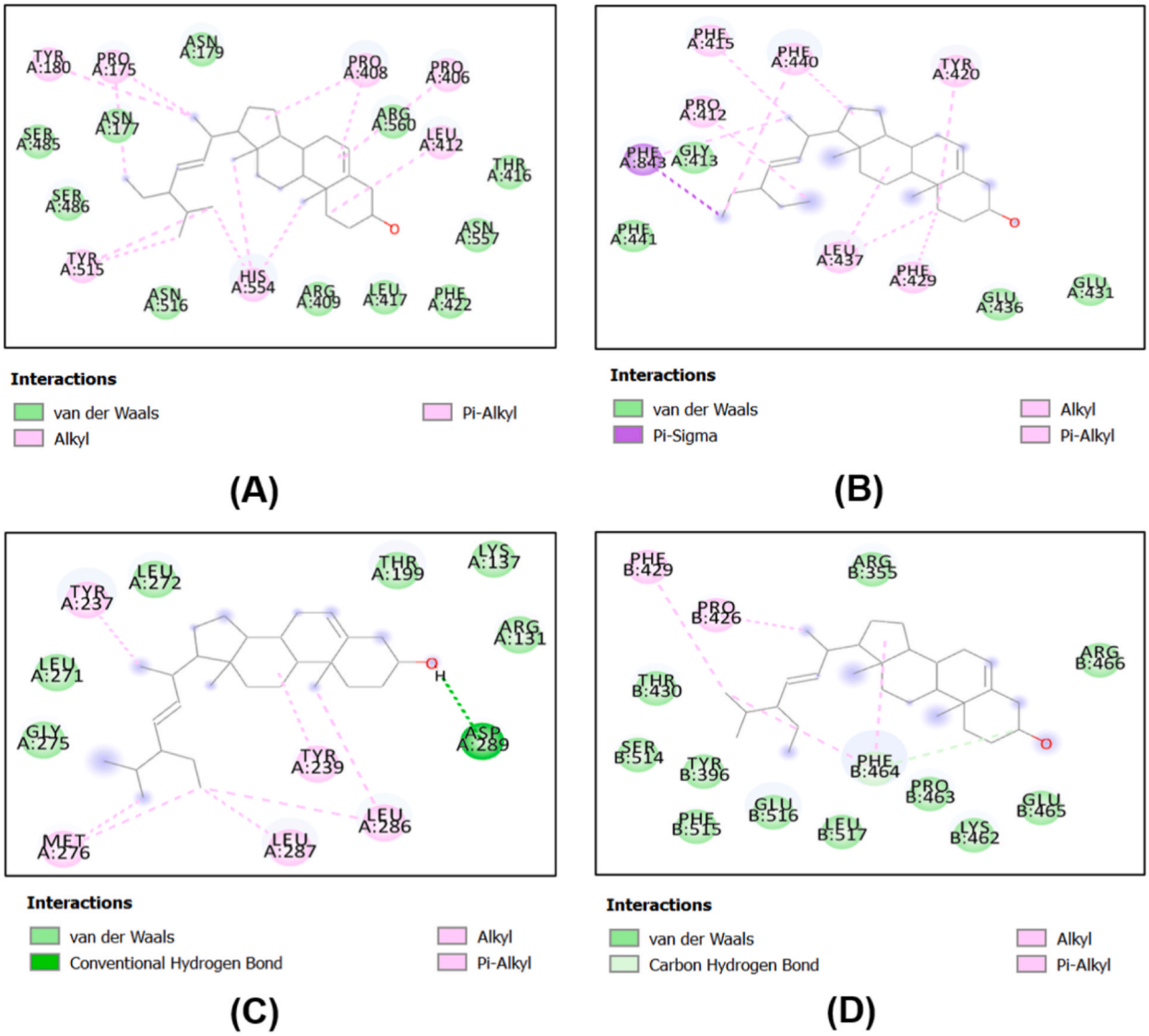

Fig. 4. The 2D visualization of the molecular interactions. (A) Stigmasterol_Helicase, (B) Stigmasterol_RdRp, (C) Stigmasterol_Mpro, (D) Stigmasterol_RBD-Spike.

Table 7
In vitro antioxidant activity of *Pterocarpus macrocarpus* Kurz. heartwood extract.

No.	Extract	Antioxidant activity, IC_{50} (μg/ml)	
		DPPH	ABTS
1	*n*-Hexane	27.70 ± 4.29	68.93 ± 4.34
2	Ethyl acetate	2.12 ± 0.97	0.75 ± 0.42
3	Ethanol	0.76 ± 0.92	0.61 ± 0.46
4	Homopterocarpin	194.90 ± 34.96	30.94 ± 8.00
5	Ascorbic acid	5.12 ± 2.43	2.77 ± 1.30
6	Trolox	0.97 ± 0.30	0.86 ± 0.97

Note: The data were represented as mean ± SD, n = 3.

Table 8
In vitro antimalarial activity, *in vitro* toxicity, and selectivity index (SI) of *Pterocarpus macrocarpus* Kurz. heartwood extracts against *P. falciparum* strain 3D7.

No	Extract	Percentage of inhibition at each concentration (μg/ml)						IC_{50} (μg/ml)	*In vitro* toxicity, CC_{50} (μg/ml)	Selectivity Index (SI)
		100	10	1	0.1	0.01	0.001			
1	*n*-Hexane	84.21	55.20	23.21	9.11	1.75	ND[a]	7.11	202.38	28.46
2	Ethyl acetate	88.26	65.99	38.12	23.28	11.54	ND	1.78	67.24	37.77
3	Ethanol	81.78	67.00	43.05	23.55	5.33	ND	2.21	512.48	231.89
4	Homopterocarpin	–	97.98	78.68	52.16	30.30	15.39	0.52	49.93	96.02
5	Chloroquine diphosphate	100.00	100.00	100.00	79.76	40.49	17.17	0.014		

[a] ND = not detectable.

Table 9
Diameter of inhibition zone and percentage of inhibition of heartwood extract of *Pterocarpus macrocarpus* Kurz.

No.	Natural Products	*Bacillus substilis*		*Candida albicans*		*Escherichia coli*		*Staphylococcus aureus*	
		DIZ (cm)	PI (%)	DIZ (cm)	PI (%)	DIZ (cm)	PI (%)	DIZ (cm)	PI (%)
1	***n*-Hexane extract**	**1.10 ± 0.10**	**39.50 ± 2.08**	**-**	**-**	**-**	**-**	**0**	**0**
2	**Ethyl Acetate extract**	**1.31 ± 0.29**	**37.9 ± 0.29**	**1.20 ± 0.08**	**29.75 ± 1.53**	**1.03 ± 0.17**	**48.82 ± 7.48**	**0**	**0**
3	**Ethanol extract**	**1.17 ± 0.17**	**38.7 ± 3.27**	**1.03 ± 0.12**	**27.40 ± 6.13**	**1.06 ± 0.17**	**57.76 ± 7.48**	**1.20 ± 0.11**	**44.78 ± 0.42**
4	**Chloramphenicol**	**3.07 ± 0.39**	**-**	**-**	**-**	**1.59 ± 0.27**	**-**	**2.39 ± 0.81**	**-**
5.	**Nystatin**			**3.65 ± 0.71**	**-**				

Note: The data are represented as mean ± SD, n = 3. DIZ: diameter of inhibition zone (cm); PI: percentage of inhibition (%); positive control: Chloramphenicol and Nystatin.

Declaration

Author contributions

Dwi Kusuma Wahyuni.: Conceived and designed the experiments, Performed the experiments; Analyzed and interpreted the data; Contributed reagents, materials, analysis tools or data; Wrote the paper.

Sumrit Wacharasindhu, Wichanee Bankeeree, Hunsa Punnapayak, Sehanat Prasongsuk: Conceived and designed the experiments; Analyzed and interpreted the data; Contributed reagents, materials, analysis tools or data; Wrote the paper.

Competing interests

The authors declare that they have no competing interests.

Data availability statement

Additional data that support the findings of this study are available from the corresponding author upon reasonable request.

Consent for publication

Not applicable.

Funding

This work was supported by the Universitas Airlangga, Contract No. 405/UN3.14/PT/2020.

Acknowledgments

The authors would like to thank Viol Dhea Kharisma and Arif Muhammad Nur Ansori for their support of the in silico anti-SARS-CoV-2 assays. The authors also would like to thanks to Natural Product Medicine Research and Development (NPMRD) laboratory, Institute of Tropical Disease (ITD), Universitas Airlangga for supporting antiplasmodial and cytotoxicity assay.

Appendix A. Supplementary data

Supplementary data to this article can be found online at https://doi.org/10.1016/j.heliyon.2023.e13644.

References

[1] WHO. Coronavirus, Covid-19) Outbreak, 2021. https://www.who.int. (Accessed 10 July 2021). accessed.
[2] WHO (World Health Organization), World Malaria Report 2020, WHO Press, Geneva, Switzerland, 2020.
[3] P.A. Kweyamba, D. Zofou, N. Efange, J.N. Assob, J. Kitau, *In vitro* and *in vivo* studies on antimalarial activity of *Commiphora africana* and *Dichrostahys cinerea* used by the Maasai in Arusha Region, Tanzania, Malar, J 18 (2019) 119–125, https://doi.org/10.1186/s12936-019-2752-8.
[4] D. Katiyar, K. Singh, M. Ali, Phytochemical and pharmacologicalprofile of *Pterocarpus marsupium*: a review, Pharma Innov. J. 5 (4) (2016) 31–39.
[5] D. Latha, D. Hrishikesh, G. Shiban, C. Chandrashekar, B.R. Bharath, *In silico, in vitro* screening of plant extracts for anti-SARS-CoV-2 activity and evaluation of their acute and sub-acute toxicity, Phytomed. Plus 2 (2022), 2100233, https://doi.org/10.1016/j.phyplu.2022.100233.
[6] B.A. Gurung, M.A. Ali, F. Al-Hemaid, M. El-Zaidy, J. Lee, In *silico* analysis of major active constituents of fingerroot (*Boesenbergia rotunda*) unveils inhibitory activities against SARS-CoV-2 main protease enzyme, Saudi J. Biol. Sci. 29 (2022) 65–74, https://doi.org/10.1016/j.sjbs.2021.11.053.
[7] I. Souid, A. Korchef, S. Souid, In *silico* evaluation of *Vitis amurensis* Rupr. Polyphenol compounds for their inhibition potency against COVID-19 main enzymes Mpro and RdRp, Saudi Pharmaceut. J. 30 (2022) 570–584, https://doi.org/10.1016/j.jsps.2022.02.014.
[8] F. Yang, X. Jiang, A. Tariq, S. Sadia, Z. Ahmed, J. Sardans, M. Aleem, R. Ullah, R.W. Bussmann, Potential medicinal plants involved in inhibiting 3CLpro activity: a practical alternate approach to combating COVID-19, J. Integr. Med. In Press (2022), https://doi.org/10.1016/j.joim.2022.08.001.
[9] M. Bourhia, F.E. Amrati, R. Ullah, A.S. Alqahtani, D. Bousta, S. Ibenmoussa, N. Khlil, Coronavirus treatments: What drugs might work against COVID-19? Nat. Prod. Commun. 15 (2020) 1–7, https://doi.org/10.1177/1934578X20945442.
[10] F.N. Idris, M.M. Nadzir, Comparative studies on different extraction methods of *Centella asiatica* and extracts bioactive compounds effects on antimicrobial activities, Antibiotics 10 (4) (2021) 457, https://doi.org/10.3390/antibiotics10040457.
[11] S. Kumari, M. Deori, R. Elancheran, J. Kotoky, R. Devi, *In vitro* and *in vivo* antioxidant, anti-hyperlipidemic properties and chemical characterization of *Centella asiatic*a (L.) extract, Front. Pharmacol. 7 (2016) 400, https://doi.org/10.3389/fphar.2016.00400.
[12] F. Kabir, M.S. Sultana, H. Kurnianta, Antimicrobial activities of grape (*Vitis vinifera* L.) pomace polyphenols as a source of naturally occurring bioactive components, Afr. J. Biotechnol. 4 (2015) 2157–2161, https://doi.org/10.5897/AJB2015.14617.
[13] H.R. Lee, M.J. Bak, W.S. Jeong, Y.C. Kim, S.K. Chung, Antioxidant properties of proanthocyanidin fraction isolated from wild Grape (*Vitis amurensis*) seed, J. Korean Soc. Appl. Biol. Chem. 52 (2009) 539–544, https://doi.org/10.3839/jksabc.2009.091.
[14] R. Jitvaropasa, S. Saenthaweesuka, N. Somparna, A. Thuppiaa, S. Sireeratawonga, W. Phoolcharoen, Antioxidant, antimicrobial and wound healing activities of *Boesenbergia rotunda*, Nat. Prod. Commun. 7 (2012) 909–912, https://doi.org/10.1177/1934578X1200700727.
[15] R. Puspitasari, A. Hafid, L. Tumewu, T.S. Wahyuni, A.A. Permanasari, A. Widyawaruyanti, Anti-hepatitis C virus activity of various Indonesian plants from balikpapan botanical garden, east borneo, Jurnal Farmasi dan Ilmu Kefarmasian Indonesia 9 (2022) 48–54, https://doi.org/10.20473/jfiki.v9i12022.
[16] N.I. Mongalo, S.S. Mashele, T.J. Makhafola, *Ziziphus mucronata* Willd. (Rhamnaceae): it's botany, toxicity, phytochemistry, and pharmacological activities, Heliyon 6 (2020), e03708, https://doi.org/10.1016/j.heliyon.2020.e03708.
[17] D.K. Wahyuni, S. Rahayu, P.R. Purnama, T.B. Saputro Suharyanto, N. Wijayanti, H. Purnobasuki, Morpho-anatomical structure and DNA barcode of *Sonchus arvensis* L, Biodiversitas 20 (2019) 2417–2426, https://doi.org/10.13057/biodiv/d200841.
[18] Md.K. Hasan, I. Ara, M.S.A. Mondal, Y. Kabir, Phytochemistry, pharmacological activity, and potential health benefits of *Glycyrrhiza glabra*, Heliyon 7 (2021), e07240, https://doi.org/10.1016/j.heliyon.2021.e07240.
[19] S. Wisittipanich, C. Khadee, P. Jintana, Shoot production of plus tree branch log and it's cutting test of *Tectona grandis* Linn and *Pterocarpus macrocarpus* Kurz, Environ. Sci. (2012) 2580.
[20] C. Hongxia, K. Xiutang, Y. Longjie, W. Chengzhang, Y. Jianzhong, Chemical component and antibacterial activity of essential oil from Myanmar *Pterocarpus macrocarpus*, Chem. Ind. For. Prod. 37 (2017) 65–72, https://doi.org/10.3969/j.issn.0253-2417.2017.06.009.
[21] W. Gao, Y. Wang, B. Basavanagoud, M.K. Jamil, Characteristics studies of molecular structures in drugs, Saudi Pharmaceut. J. 25 (2017) 580–586, https://doi.org/10.1016/j.jsps.2017.04.027.
[22] J. Chen, S. Ge, Z. Liu, W. Peng, GC-MS explores health care components in the extract of *Pterocarpus macrocarpus* Kurz, Saudi J. Biol. Sci. 25 (2018) 1196–1201, https://doi.org/10.1016/j.sjbs.2017.12.013.
[23] S. Ataa, I.R. Hazmi, S.F. Samsudin, Insect's visitation on *Melastoma malabathricum* in UKM Bangi forest reserve, EES (Ecotoxicol. Environ. Saf.) 1 (2017) 20–22, https://doi.org/10.26480/ees.01.2017.22.24.
[24] M. Morimoto, H. Fukumoto, M. Hiratani, W. Chavasiri, K. Komai, Insect antifeedants, pterocarpans, and pterocarpol, in heartwood of *Pterocarpus macrocarpus* Kurz, Biosci. Biotechnol. Biochem. 70 (2014) 1864–1868, https://doi.org/10.1271/bbb.60017.
[25] L.K. Hanoon, S.D.S.D. Joshi, A.K. Yasir, A.M. Prasad, K.S. Alapati, Phytochemical screening and antioxidant activity of Pseuderanthemum malabaricum, J. Pharmacogn. Phytochem. 8 (2019) 972–977.
[26] V. Rashida, A.R. Nisha, Phytochemical and chromatographic analysis of flavonoid fraction isolated from methanolic extract of *Pterocarpus marsupium*, J. Phytopharm. 11 (2022) 79–88.
[27] D.K. Wahyuni, S. Rahayu, A.H. Zaidan, W. Ekasari, S. Prasongsuk, H. Purnobasuki, Growth, secondary metabolite production, and *in vitro* antiplasmodial activity of *Sonchus arvensis* L. callus under dolomite [$CaMg(CO_3)_2$] treatment, PLoS One 16 (2021), e0254804, https://doi.org/10.1371/journal.pone.0254804.
[28] V.D. Kharisma, A.N.M. Ansori, A.P. Nugraha, Computational study of ginger (*Zingiber officinale*) as E6 inhibitor in human papillomavirus type 16 (HPV-16) infection, Biochem. Cell. Arch. 20 (2020) 3155–3159, https://doi.org/10.35124/bca.2020.20.S1.3155.
[29] Y.B. Choy, M.R. Prausnitz, The rule of five for non-oral routes of drug delivery: ophthalmic, inhalation and transdermal, Pharm. Res. (N. Y.) 28 (2011) 943–948, https://doi.org/10.1007/s11095-010-0292-6.
[30] W.E. Putra, V.D. Kharisma, H. Susanto, Potential of *Zingiber officinale* bioactive compounds as inhibitory agent against the IKK-B, AIP Conf. Proc. 2231 (2020), 040048, https://doi.org/10.1063/5.0002478.
[31] C. Prahasanti, A.P. Nugraha, V.D. Kharisma, A.N.M. Ansori, R. Devijanti, T.P.S.P. Ridwan, N.F. Ramadhani, I.B. Narmada, I.G.A.W. Ardani, T.N.E.B.A. Noor, A bioinformatics approach of hydroxyapatite and polymethylmethacrylate composite exploration as dental implant biomaterial, J. Pharm. Pharmacogn. Res. 9 (2021) 746–754.
[32] R.M. Wijaya, M.A. Hafidzhah, V.D. Kharisma, A.N.M. Ansori, A.A. Parikesit, COVID-19 in silico drug with *Zingiber officinale* natural product compound library targeting the Mpro protein, Makara J. Sci. 25 (2021) 162–171, https://doi.org/10.7454/mss.v25i3.1244.
[33] L. Vania, M.H. Widyananda, V.D. Kharisma, A.N.M. Ansori, S.W. Naw, N. Maksimiuk, M. Derkho, A. Denisenko, N.I. Sumantri, A.P. Nugraha, Anti-cancer activity prediction of *Garcinia mangostana* L. againts her2-positive breast cancer through Inhibiting EGFR, HER2 and IGF1R protein: a bioinformatics study, Biochem. Cell. Arch. 21 (2021) 3313–3321.
[34] J.M. Prieto, in: Procedure: Preparation of DPPH Radical, and Antioxidant Scavenging Assay. Prieto's DPPH Microplate Protocol, 2012 (accessed March 30, 2021), https://www.researchgate.net/-file.PostFileoader.html?id=503cd1c9e39d5ead11000043&assetKey=AS%3A271744332435456%401441800305338.
[35] R. Fu, Y. Zhang, Y. Guo, F. Liu, F. Chen, Determination of phenolic contents and antioxidant activities of extracts of *Jatropha curcas* L. seed shell, a by-product, a new source of natural antioxidant, Ind. Crop. Prod. 58 (2014) 265–270, https://doi.org/10.1016/j.indcrop.2014.04.031.

[36] D.K. Wahyuni, H. Purnobasuki, E.P. Kuncoro, W. Ekasari, Callus induction of *Sonchus arvensis* L. and its antiplasmodial activity, Afr. J. Infect. 14 (2020) 1–7, https://doi.org/10.21010/ajid.v14i1.1.

[37] A.G. Fonseca, L.L.S.F.R. Dantas, J.M. Fernandes, S.M. Zucolotto, A.A.N. Lima, L.A.L. Soares, H.A.O. Rocha, T.M.A.M. Lemos, *In vivo* and *in vitro* toxicity evaluation of hydroethanolic extract of *Kalanchoe brasiliensis* (Crassulaceae) Leaves, J. Toxicol. 6849765 (2018) 1–8, https://doi.org/10.1155/2018/6849765.

[38] R.J. Ferreira, M. Gajdács, A. Kincses, G. Spengler, D.J.V.A. dos Santos, M.U. Ferreira, Nitrogen-containing naringenin derivatives for reversing multidrug resistance in cancer, Bioorg. Med. Chem. 28 (2020), 115798, https://doi.org/10.1016/j.bmc.2020.115798.

[39] G.E. de Souza, R.V. Bueno, J.O. de Souza, C.L. Zanini, F.C. Cruz, G. Oliva, R.C. Guido, A.C.A. Caroline, Antiplasmodial profile of selected compounds from Malaria Box: *In vitro* evaluation, speed of action and drug combination studies, Malar. J. 18 (2019) 447–459, https://doi.org/10.1186/s12936-019-3069-3.

[40] A. Yadav, M. Yadav, S. Kumar, J.P. Yadav, Bactericidal effect of *Acacia nilotica: in vitro* antibacterial and time-kill kinetic studies, Int. J. Curr. Res. 7 (2015) 22289–22294.

[41] M.E. Abouelela, R.A. Abdelhamid, M.A.A. Orabi, Phytochemical constituents of plant species of Pterocarpus (F: leguminosae): a review, Int. J. Pharmacogn. Phytochem. Res. 11 (2019) 264–281.

[42] D. Arbain, G.A. Saputri, G.S. Syahputra, Y. Widiyastuti, D. Susanti, M. Taher, Genus Pterocarpus: a review of ethnopharmacology, phytochemistry, J. Ethnopharmacol. 278 (2021), 114316, https://doi.org/10.1016/j.jep.2021.114316.

[43] U. Usunomena, I.V. Chinwe, Phytochemical screening, mineral composition, and *in vitro* antioxidant activities of *Pterocarpus mildbraedii* leaves, Int. J. Sci. World 4 (2016) 23–26, https://doi.org/10.14419/ijsw.v4i1.6066.

[44] T. Ahamed, S.K.M. Rahman, A.M. Shohae, Thin-layer chromatographic profiling and phytochemical screening of six medicinal plants in Bangladesh, Int. J. Biosci. 11 (2017) 131–140.

[45] W.A. Yehye, N.A. Rahman, A.A. Alhadi, H. Khaledi, S.W. Ng, A. Ariffin, Butylated hydroxytoluene analogs: synthesis and evaluation of their multipotent antioxidant activities, Molecules 17 (2012) 7645–7665.

[46] M.A. Zeb, S.U. Khan, T.U. Rahman, M. Sajid, S. Seloni, Isolation and biological activity of β-sitosterol and stigmasterol from the roots of Indigofera heterantha, PPIJ 5 (2017) 204–207.

[47] P. Sirikhansaeng, T. Tanee, R. Sudmoon, A. Chaveerach, Major phytochemical as γ-sitosterol disclosing and toxicity testing in Lagerstroemia species, Evid.-based Complement, Altern. (2017), 7209851, https://doi.org/10.1155/2017/7209851.

[48] A.C. Akinmoladun, T.M. Olaleye, K. Komolafe, A.O. Adetuyi, Effect of homopterocarpin, an isoflavonoid from Pterocarpus erinaceus, on indices of liver injury and oxidative stress in acetaminophen-provoked hepatotoxicity, JBCPP 26 (2015) 555–562, https://doi.org/10.1515/jbcpp-2014-0095.

[49] O. Fiehn, Metabolomics by gas chromatography-mass spectrometry: the combination of targeted and untargeted profiling, Curr. Protoc. Mol. Biol. 114 (2016) 30.4.1–30.4.32, https://doi.org/10.1002/0471142727.mb3004s114.

[50] National Institutes of Health, National Library of Medicine, National Center for Biotechnology Information., Homopterocarpin, 2021. https://pubchem.ncbi.nlm.-nih.gov/compound/-Homopterocarpin. (Accessed 9 August 2021). accessed.

[51] I. Abdelli, F. Hassani, S.B. Brikci, S. Ghalem, *In silico* study the inhibition of angiotensin converting enzyme 2 receptor of COVID-19 by *Ammoides verticillata* components harvested from Western Algeria, J. Biomol. Struct. Dyn. 39 (2021) 3263–3276, https://doi.org/10.1080/07391102.2020.1763199.

[52] A. Hassan, Z. Akmal, N. Khan, The phytochemical screening and antioxidants potential of *Schoenoplectus triqueter* L, Palla. J. Chem. (2020), 3865139, https://doi.org/10.1155/2020/3865139.

[53] M.A. Yahya, I.H. Nurrosyidah, Antioxidant activity ethanol extract of gotu kola (Centella asiatica L.) with DPPH method (2,2-diphenyl-1-pikrilhidrazil), J. Halal Prod. Res. 3 (2020) 106–112, https://doi.org/10.20473/jhp.

[54] A.K. Esmaeili, R.M. Taha, S. Mohajer, B. Banisalam, Antioxidant activity and total phenolic and flavonoid content of various solvent extracts from *in vivo* and *in vitro* grown *Trifolium pratense* L. (Red Clover), BioMed Res. Int. 643285 (2015) 1–11, https://doi.org/10.1155/2015/643285.

[55] D.N. Olennikov, I.N. Zilfikarov, A.A. Toropova, T.A. Ibragimov, Chemical composition of *Callisia fragrans* wood juice and its antioxidative activity (*in vitro*), Chem. Plant Raw Mater. 4 (2008) 95–100, https://doi.org/10.1007/s10600-009-9174-8.

[56] H.C. Upadhyaya, B.S. Sisodia, H.S. Cheema, J. Agrawal, A. Pal, M.P. Darokar, S.K. Srivastava, Novel antiplasmodial agents from *Christia vespertilionis*, Nat. Prod. Commun. 8 (2013) 1591–1594, https://doi.org/10.1177/1934578X1300801123.

[57] P. Chaniad, A. Phuwajaroanpong, T. Techarang, P. Viriyavejakul, A. Chukaew, C. Punsawad, Antiplasmodial activity and cytotoxicity of plant extracts from the Asteraceae and Rubiaceae families, Heliyon 8 (2022), e08848, https://doi.org/10.1016/j.heliyon.2022.e08848.

[58] O. Noufou, T. André, S.W. Richard, S. Yerbanga, T. Maminata, S. Ouédraogo, E.H. Anne, G. Irène, G.I. Pierre, Anti-inflammatory and anti-plasmodial activities of methanol extract of *Pterocarpus erinaceus* Poir. (Fabaceae) leaves, Int. J. Pharmacol. 89 (2016) 291–294, https://doi.org/10.3923/ijp.2016.549.555.

[59] N. Tajuddeen, N. van Heerden, Antiplasmodial natural products: an update, Malar. J. 18 (2019) 1–62, https://doi.org/10.1186/s12936-019-3026-1.

[60] S. Sinha, D.I. Batovska, B. Medhi, B.D. Radotra, A. Bhalla, N. Markova, R. Sehgal, *In vitro* anti-malarial eficacy of chalcones: cytotoxicity profile, mechanism of action and their efect on erythrocytes, Malar. J. 18 (2019) 421–432, https://doi.org/10.1186/s12936-019-3060-z.

[61] R.A. Safitri, O. Saptarini, T. Sunarni, Cytotoxic activity, expression of p53, and Bcl-2 extract fraction of Kelakai Herbs (*Stenochleana palustris* (Burm.F.) Bedd.) to breast cancer T47D cells, Jurnal Biotek Medisiana Indonesia 9 (2020) 113–127.

[62] E.S. Omoregie, A. Pal, B. Sisodia, *In vitro* antimalarial and cytotoxic activities of leaf extracts of *Vernonia amygdalina* (Del.), Nig. J. Basic Appl. Sci. 19 (2011) 121–126, https://doi.org/10.4314/njbas.v19i1.69356.

[63] S.N. Njeru, J.M. Muema, Antimicrobial activity, phytochemical characterization and gas chromatography-mass spectrometry analysis of *Aspilia pluriseta* Schweinf. extracts, Heliyon 6 (2020), e05195, https://doi.org/10.1016/j.heliyon.2020.e05195.

[64] N.P. Mangalagiri, S.K. Panditi, N.L.L. Jeevigunta, Antimicrobial activity of essential plant oils and their major components, Heliyon 7 (2021), e06835, https://doi.org/10.1016/j.heliyon.2021.e06835.

[65] F.G. Saqallah, W.H. Hamed, W.H. Talib, R. Dianita, H.A. Wahab, Antimicrobial activity and molecular docking screening of bioactive components of *Antirrhinum majus* (snapdragon) aerial parts, Heliyon 8 (2022), e10391, https://doi.org/10.1016/j.heliyon.2022.e10391.

[66] S. Saivaraj, G. Chandramohan, Antimicrobial activity of natural dyes obtained from *Pterocarpus indicus* Willd. bark, Asian J. Pharmaceut. Res. Dev. 6 (2018) 6–8, https://doi.org/10.22270/ajprd.v6i2.363.

[67] L. Jime′nez-Gonza′lez, M.A. lvarez-Corral, M. Muñoz-Dorado, I. Rodrı′guez-Garcı′a, Pterocarpans: interesting natural products with antifungal activity and other biological properties, Phytochemistry Rev. 7 (2008) 125–154, https://doi.org/10.1007/s11101-007-9059-z.

[68] J.E. Cuellar, J. Martínez, B. Rojano, J.H. Gil, D. Durango, Chemical composition and antioxidant and antibacterial activity of *Platymiscium gracile* Benth.: a species threatened by extinction, J. King Saud Univ. Sci. 32 (2020) 702–708, https://doi.org/10.1016/j.jksus.2018.11.006.

[69] G. Gutie′rrez-Venegas, J.A. Go′mez-Mora, M.A. Meraz-Rodríguez, M.A. Flores-Sa′nchez, L.F. Ortiz-Miranda, Effect of flavonoids on antimicrobial activity of microorganisms present in dental plaque, Heliyon 5 (2019), e03013, https://doi.org/10.1016/j.heliyon.2019.e03013.

[70] A.P. Wardana, N.S. Aminah, M. Rosyda, M.I. Abdjan, A.N. Kristanti, K.N.W. Tun, M.I. Choudhary, Y. Takaya, Potential of diterpene compounds as antivirals, a review, Heliyon 7 (2021), e06515, https://doi.org/10.1016/j.heliyon.2021.e07777.